Nano-Micro Letters

Supporting Information for

Targeting Hypoxic Tumors with Hybrid Nanobullets for Oxygen-Independent Synergistic Photothermal and Thermodynamic Therapy

Di Gao[1, †], Ting Chen[1, †], Shuojia Chen[1], Xuechun Ren[1], Yulong Han[2, 3], Yiwei Li[2, 3], Ying Wang[1], Xiaoqing Guo[1], Hao Wang[1], Xing Chen[4], Ming Guo[3], Yu Shrike Zhang[5], Guosong Hong[6], Xingcai Zhang[2,3, *], Zhongmin Tian[1, *], Zhe Yang[1, *]

[1]The Key Laboratory of Biomedical Information Engineering of Ministry of Education, School of Life Science and Technology, Xi'an Jiaotong University, Xi'an 710049, P. R. China

[2]John A. Paulson School of Engineering and Applied Sciences, Harvard University, Cambridge, Massachusetts 02138, United States

[3]School of Engineering, Massachusetts Institute of Technology, Cambridge, MA, 02139, United States

[4]School of Public Health, Guangxi Medical University, Nanning 530000, P. R. China

[5]Division of Engineering in Medicine, Department of Medicine, Brigham and Women's Hospital, Harvard Medical School, Cambridge, MA, 02139, United States

[6]Department of Materials Science and Engineering, Stanford University, Stanford, CA 94305, United States

† Di Gao and Ting Chen contributed equally to this work

*Corresponding author. E-mail: yangzhe@xjtu.edu.cn (Zhe Yang) zmtian@mail.xjtu.edu.cn (Zhongmin Tian) or xingcai@mit.edu (Xingcai Zhang)

Supplementary Tables and Figures

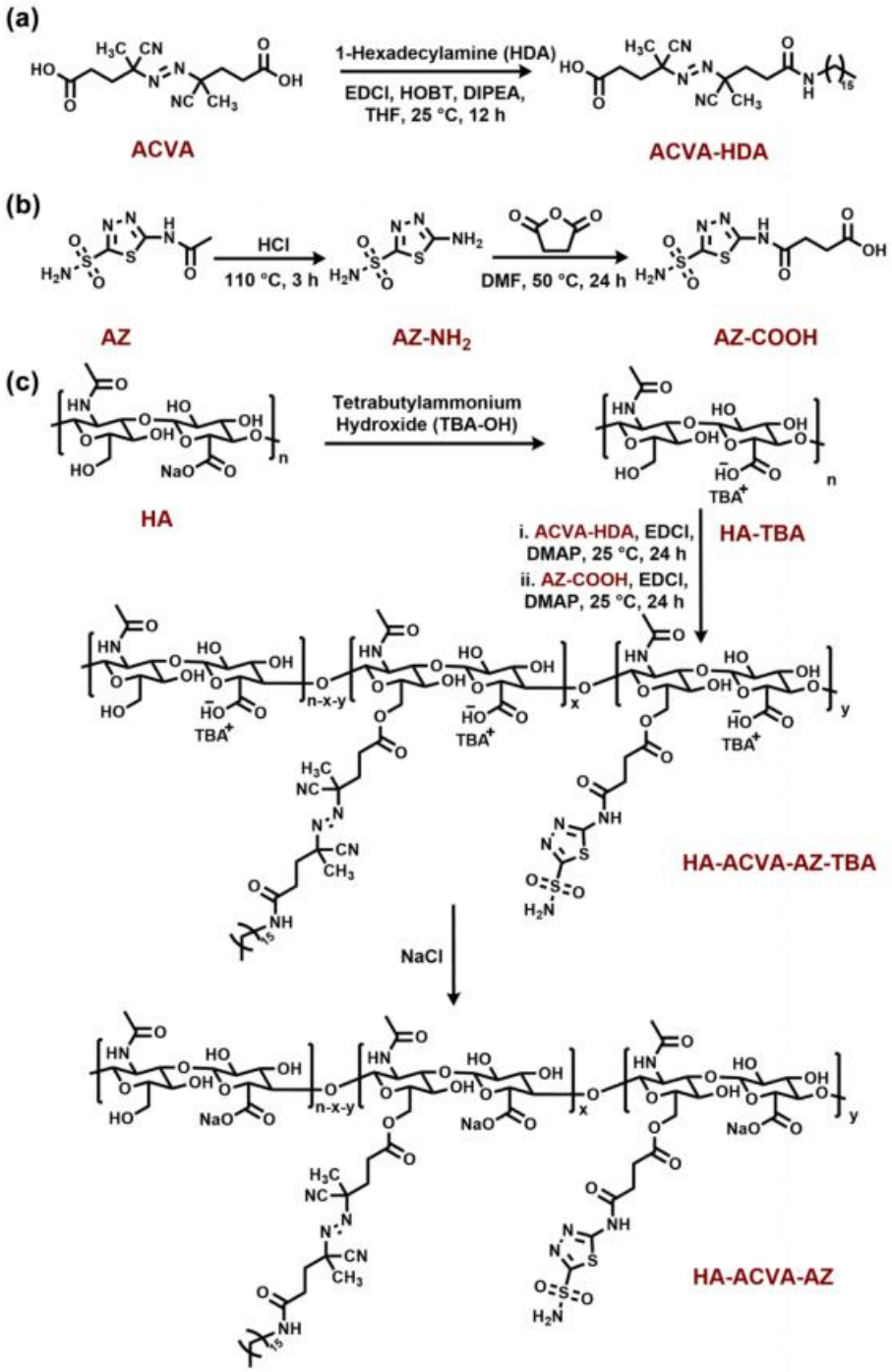

Fig. S1 a Synthesis of ACVA-HDA. **b** Synthesis of AZ-COOH. **c** Synthetic route of the amphiphilic polymer HA-ACVA-AZ

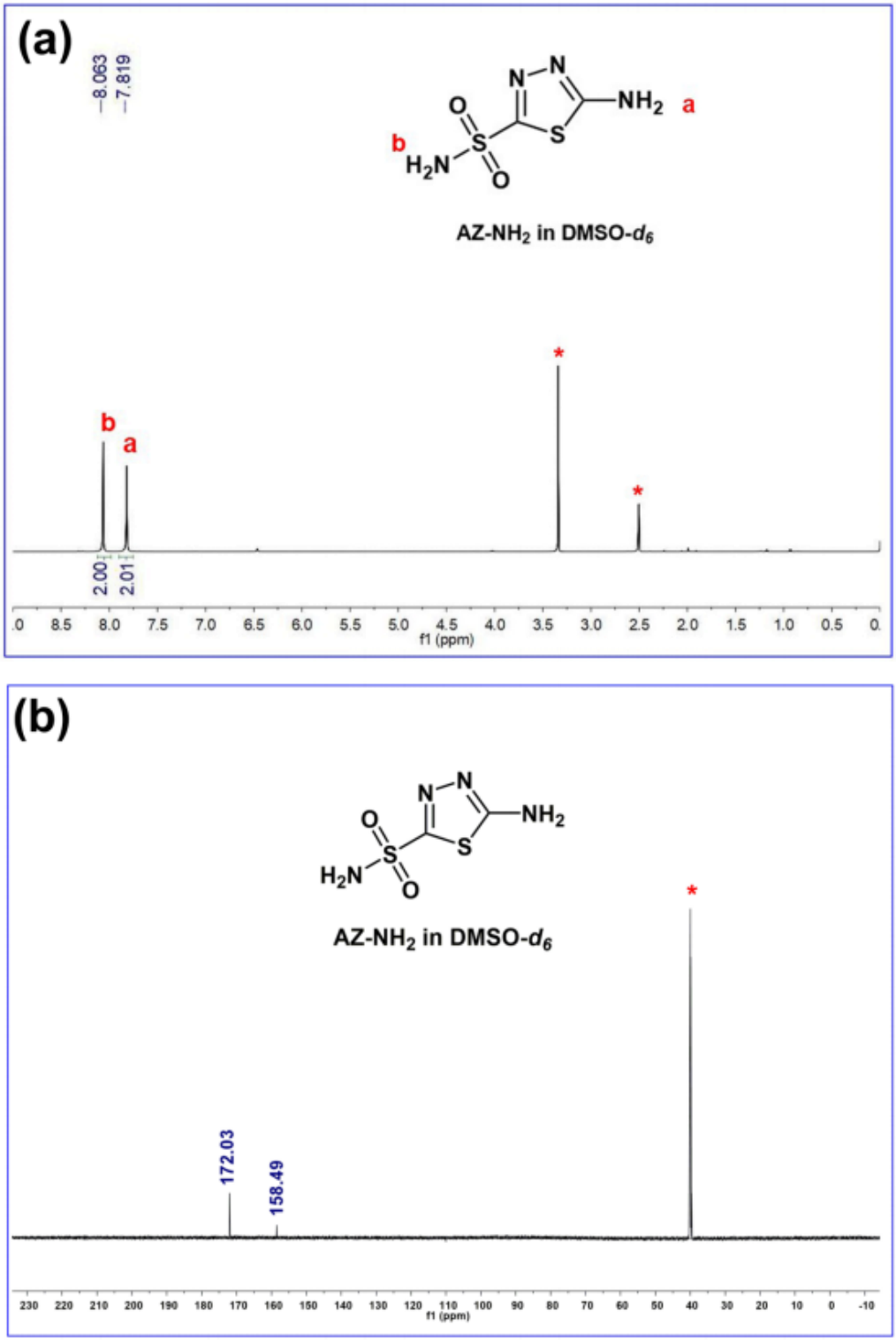

Fig. S2 a ^{1}H NMR and **b** ^{13}C {^{1}H} NMR spectrum of AZ-NH_2 in DMSO-d_6

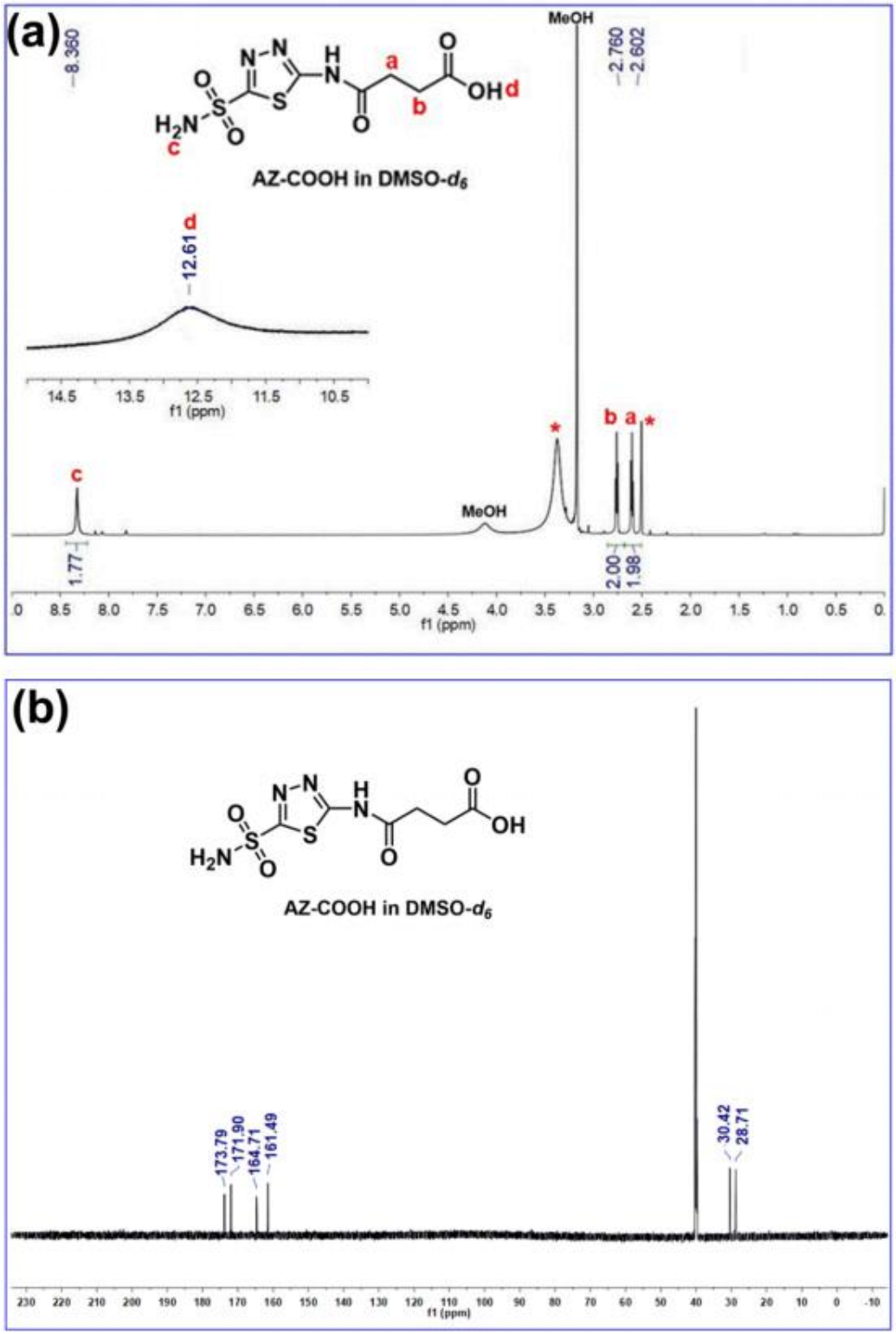

Fig. S3 a ^{1}H NMR and **b** ^{13}C {^{1}H} NMR spectrum of AZ-COOH in DMSO-d_6

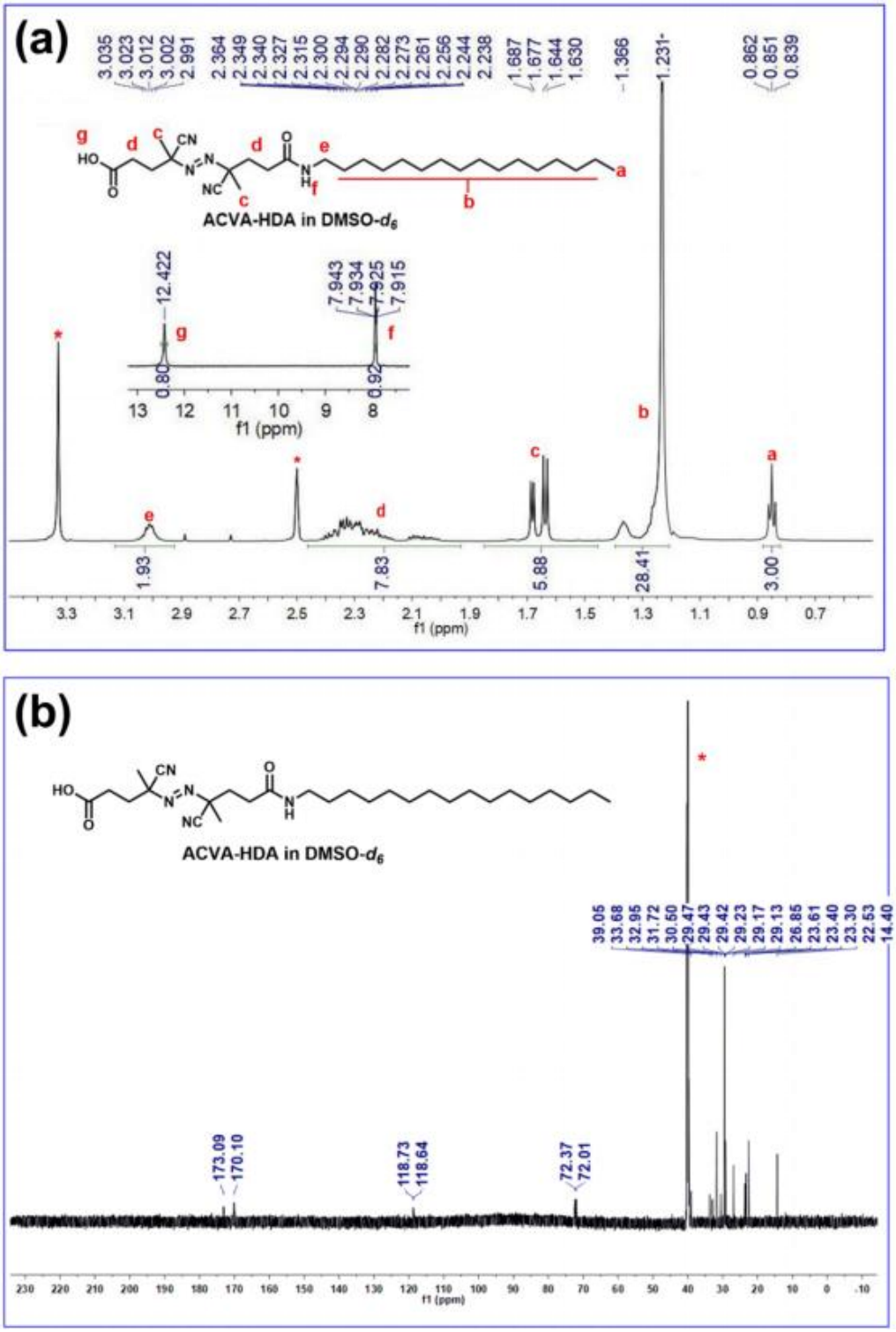

Fig. S4 a ^{1}H NMR and **b** ^{13}C {^{1}H} NMR spectrum of ACVA-HDA in DMSO-d_6

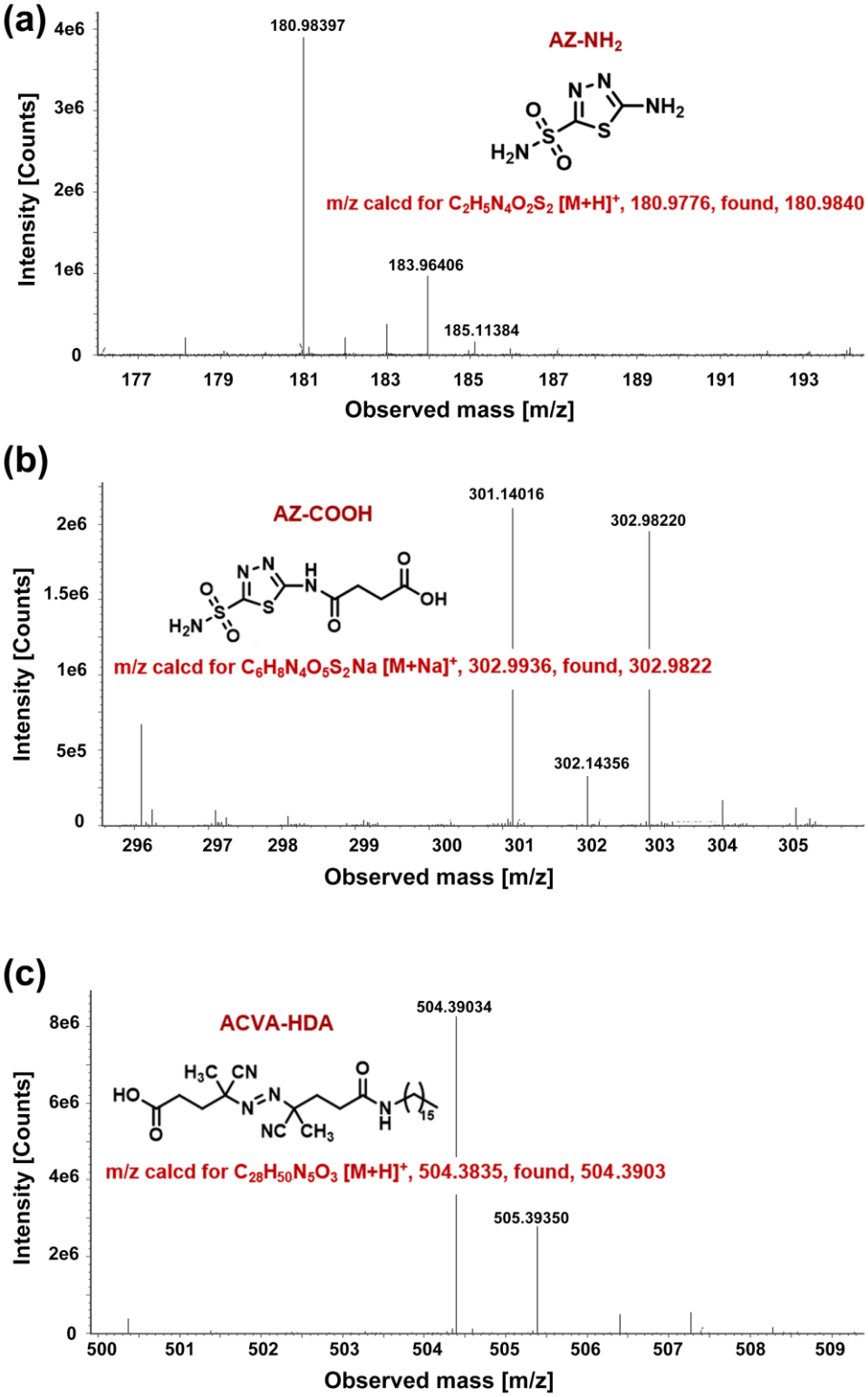

Fig. S5 ESI mass spectrum: **a** AZ-NH_2, **b** AZ-COOH, **c** ACVA-HDA

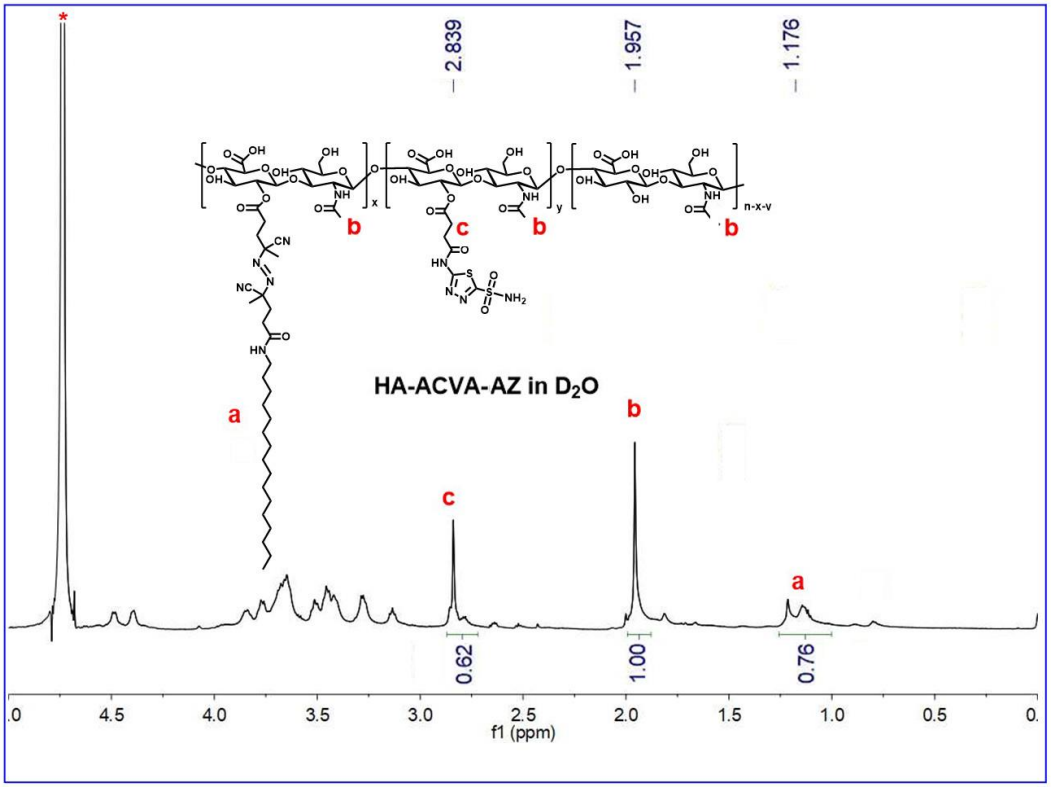

Fig. S6 ^{1}H NMR spectrum of HA-ACVA-AZ in D_2O

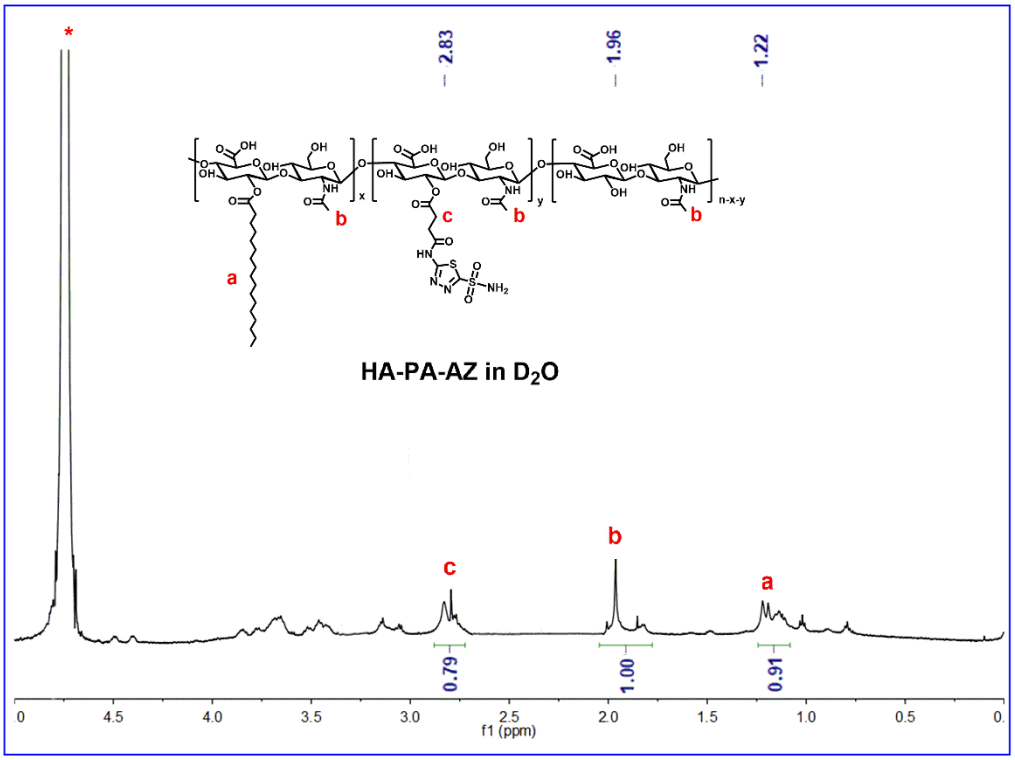

Fig. S7 ^{1}H NMR spectrum of HA-PA-AZ in D_2O

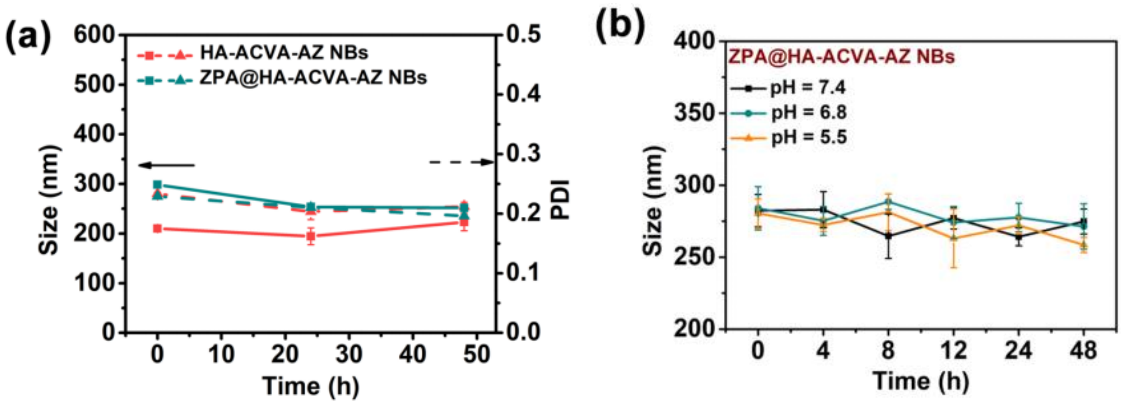

Fig. S8 **a** Changes of HA-ACVA-AZ NBs' and ZPA@HA-ACVA-AZ NBs' size and PDI in PBS containing FBS (10%, v/v) at 37 °C for 48 h. **b** Changes of HA-ACVA-AZ NBs' and ZPA@HA-ACVA-AZ NBs' size in different PBS (pH 7.4, 6.8 and 5.5) at 37 °C for 48 h. Data are shown as the mean ± standard deviation (n = 3)

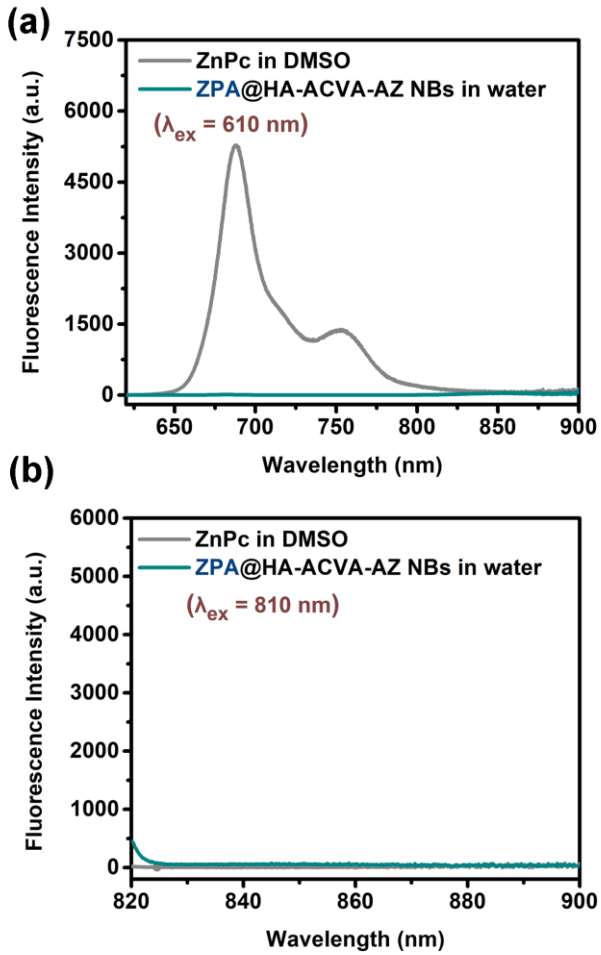

Fig. S9 Fluorescence spectra of ZPA@HA-ACVA-AZ NBs in deionized water and ZnPc in DMSO with excitation wavelength at **a** 610 nm and **b** 810 nm ([ZnPc] = 10 μM)

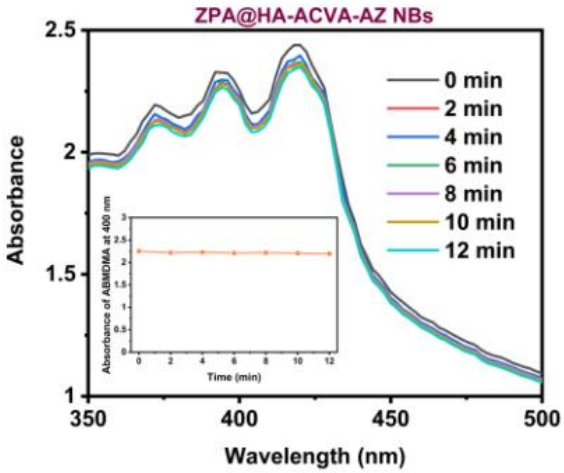

Fig. S10 Change in absorption spectrum of ABMDMA in deionized water in the presence of ZPA@HA-ACVA-AZ NBs upon laser irradiation (808 nm, 1 W cm^{-2}, [ZnPc] = 5 μM). The inset shows the variation of absorbance at 400 nm with time

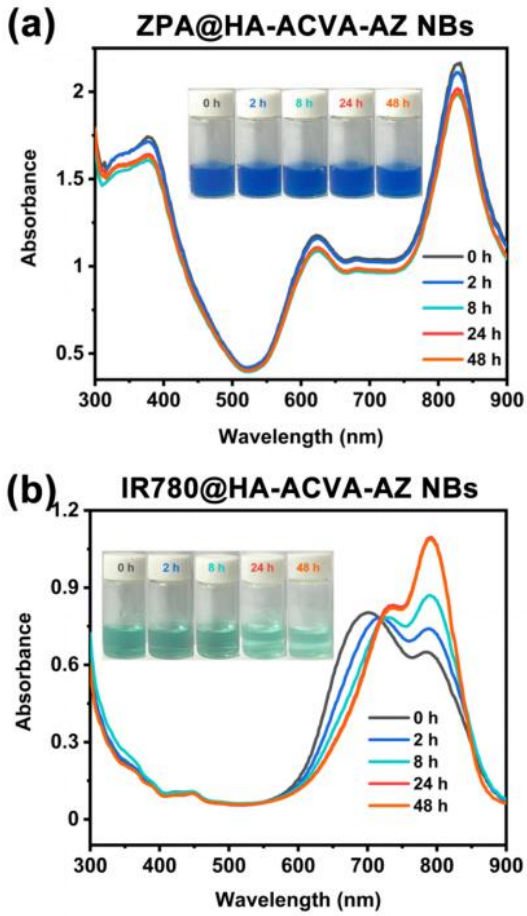

Fig. S11 Change in the absorption spectrum of **a** ZPA@HA-ACVA-AZ NBs and **b** IR780@HA-ACVA-AZ NBs in PBS (pH = 7.4) at 37 °C over time

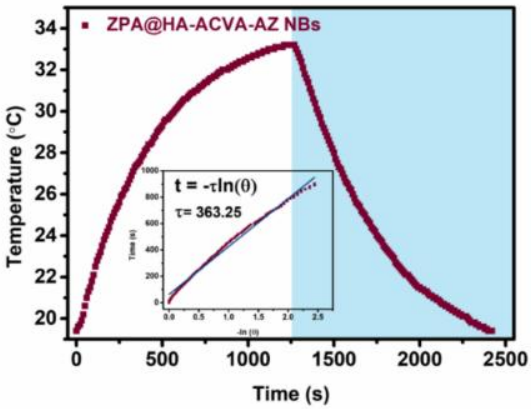

Fig. S12 Photothermal profile of ZPA@ HA-ACVA-AZ NBs in deionized water irradiated by 808 nm NIR laser ([ZnPc] = 20 μM, 1 W/cm^2) for 21 min, followed by natural cooling to room temperature. (Inset figure: determination of time constant for heat transfer (τ) of the system)

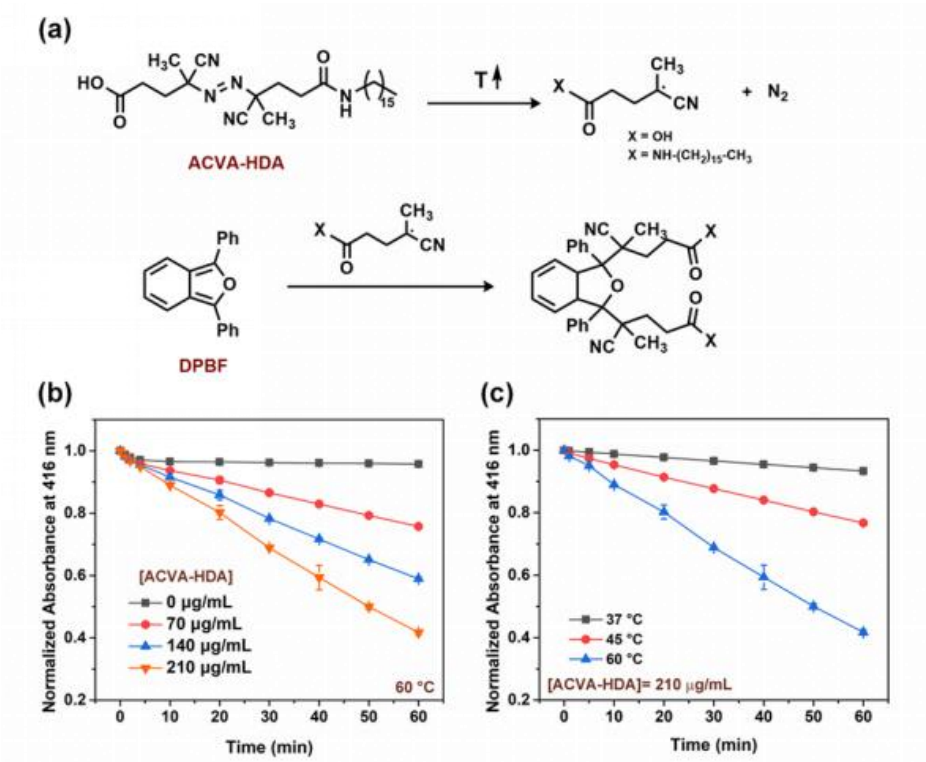

Fig. S13 a The mechanism for the degradation of DPBF by alkyl radicals upon heating ACVA-HDA. **b** Degradation rate of DPBF sensitized by ACVA-HDA in DMF of different concentrations at 60 °C. **c** Degradation rate of DPBF sensitized by ACVA-HDA in DMF under various temperatures at concentration of 210 μg/mL

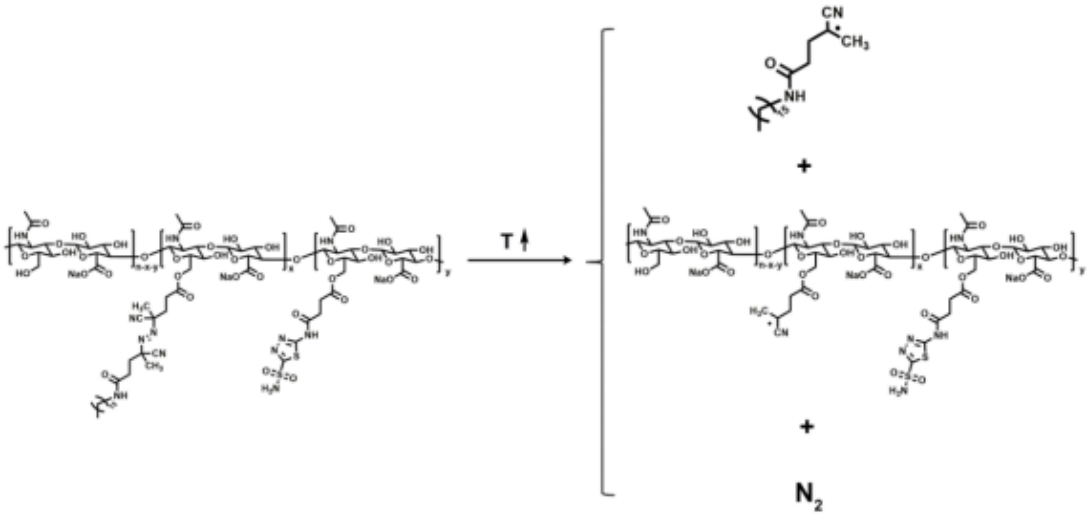

Fig. S14 Illustration of the principle and process of free radical generation upon heat treatment of HA-ACVA-AZ

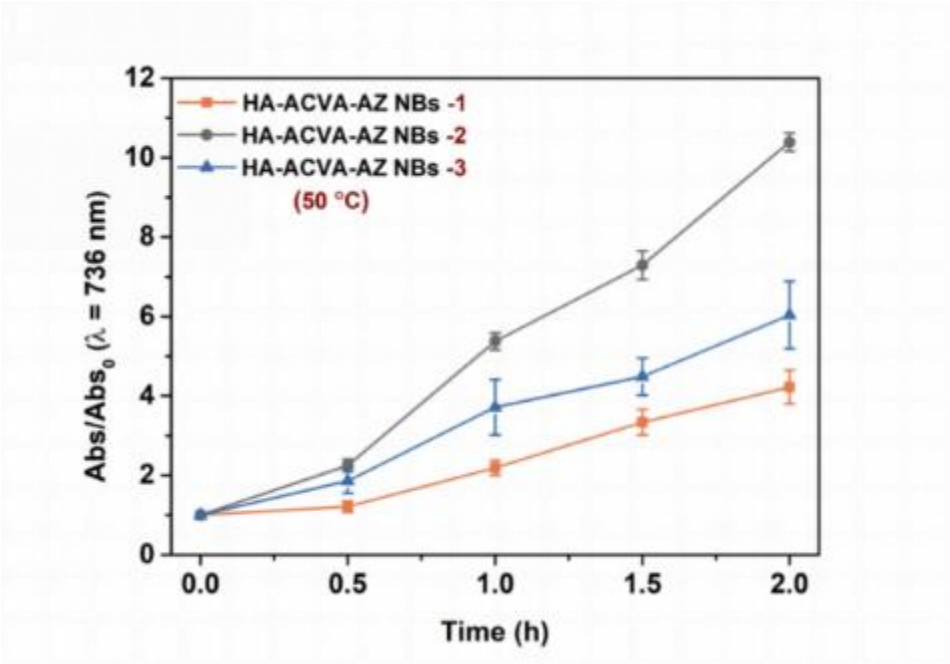

Fig. S15 Generation of $ABTS^{+\bullet}$ as induced by the free radicals released from different blank HA-ACVA-AZ NBs at 50 °C ([NBs] = 5 mg/mL)

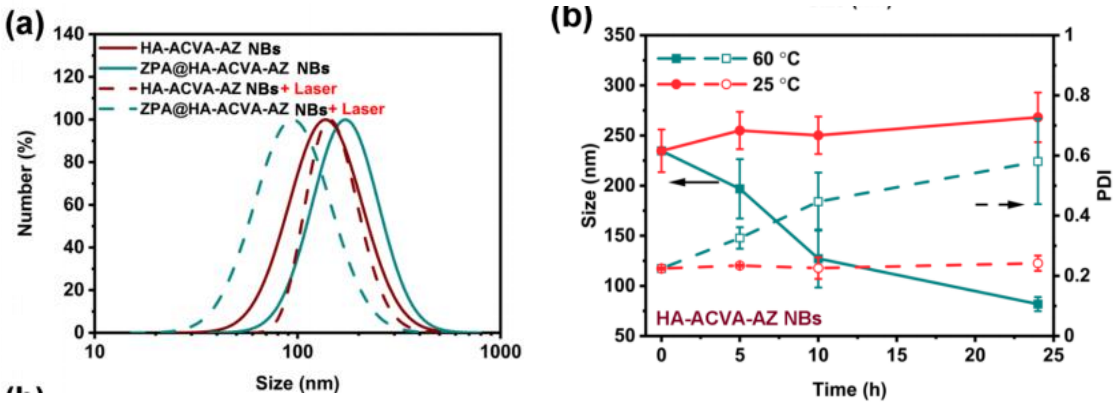

Fig. S16 a Particle size distribution of blank HA-ACVA-AZ NBs and ZPA@HA-ACVA-AZ NBs with or without laser irradiation (808 nm, 1 W/cm^2, 10 min). **b** Change in the size and PDI of blank HA-ACVA-AZ NBs at 25 °C and 60 °C over time

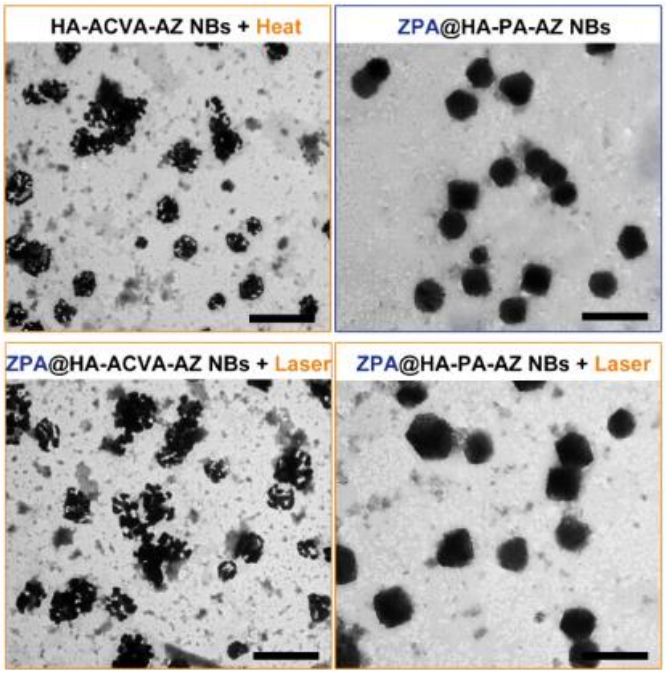

Fig. S17 TEM images of blank HA-ACVA-AZ NBs upon heat treatment, ZPA@HA-ACVA-AZ NBs with laser irradiation and ZPA@HA-PA-AZ NBs with or without laser irradiation. (scale bar: 500 nm)

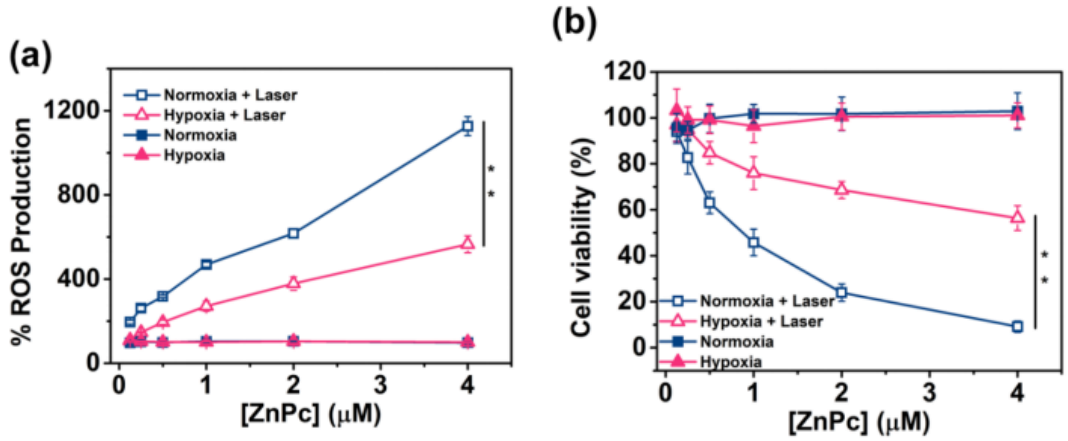

Fig. S18 **a** ROS production induced by ZnPc in 4T1 cells in the absence (closed symbols) or presence (open symbols) of 635 nm laser irradiation (30 mW/cm^2, 5 min) under normoxia or hypoxia conditions. **b** Cytotoxicity induced by ZnPc on 4T1 cell in the absence (closed symbols) or presence (open symbols) of 635 nm laser irradiation (30 mW/cm^2, 5 min) under normoxic or hypoxic conditions

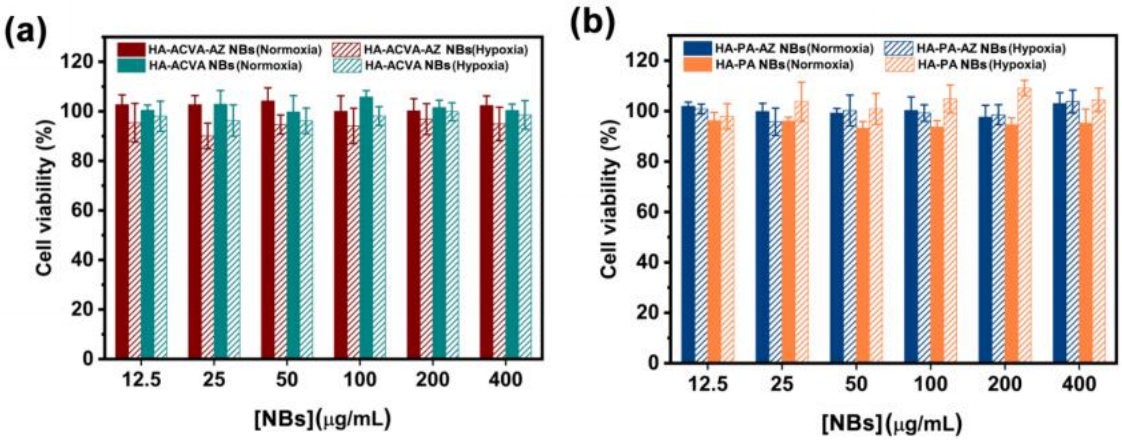

Fig. S19 Cell viability of 4T1 cells after incubation with various concentrations of **a** HA-ACVA NBs and HA-ACVA-AZ NBs, **b** HA-PA NBs and HA-PA-AZ NBs for 24 h in normoxic and hypoxic conditions

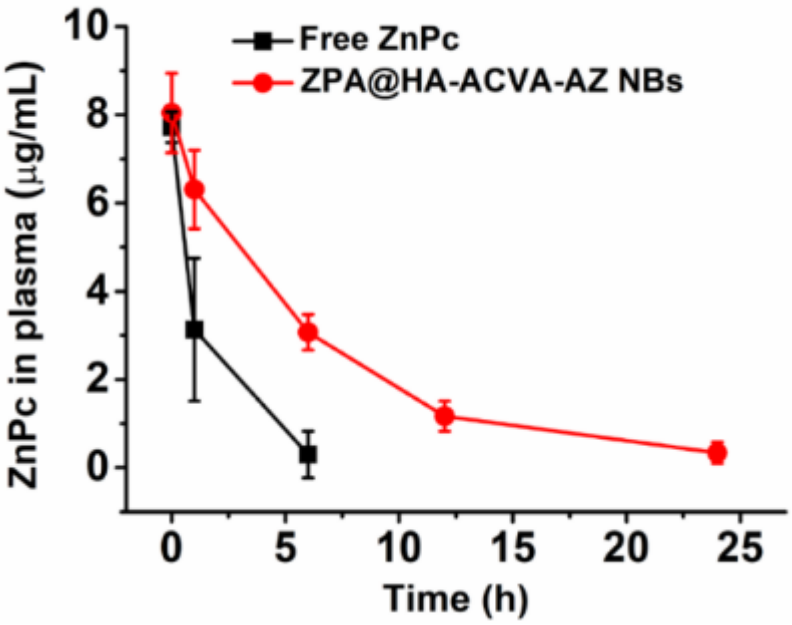

Fig. S20 Plasma ZnPc concentration versus time after intravenous administration of Free ZnPc and ZPA@HA-ACVA-AZ NBs for 24 h at an equivalent dose of 2 mg ZnPc per kg of mice body (n=5)

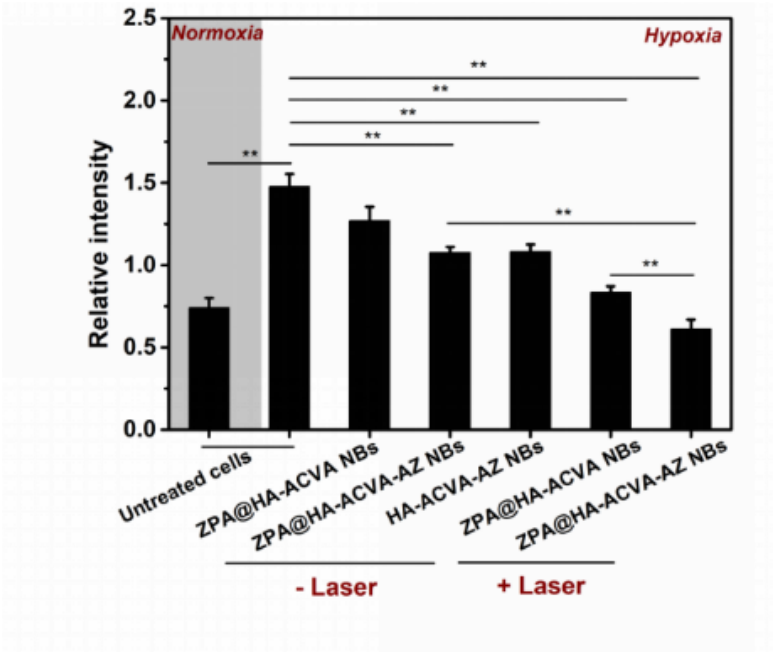

Fig. S21 Quantitative analysis of the western blotting bands for CA IX expression of 4T1 cells treated with varying drug formulations with or without 808 nm laser irradiation (1 W/cm^2, 10 min) by using ImageJ

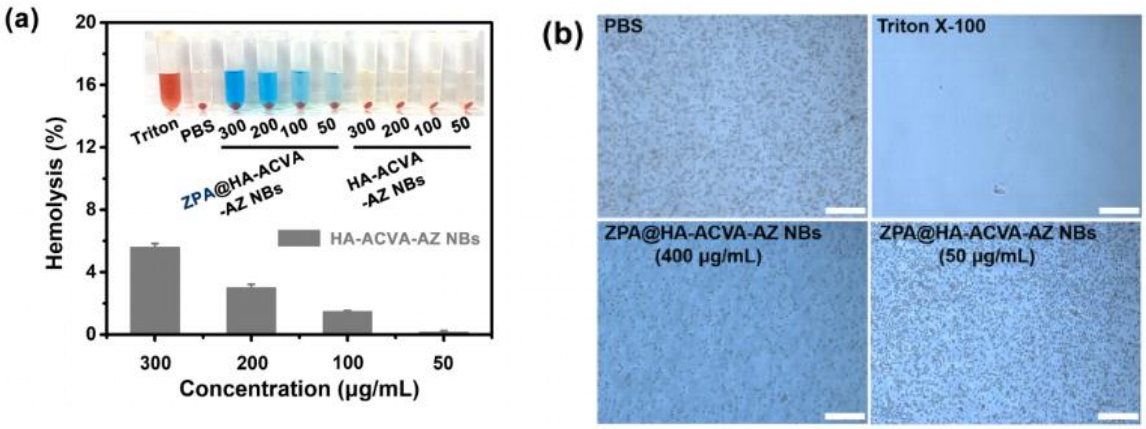

Fig. S22 a Hemolytic activity of HA-ACVA-AZ NBs at different concentrations. The inset shows the images of erythrocyte incubated with HA-ACVA-AZ NBs and ZPA@HA-ACVA-AZ NBs after centrifugation. **b** Erythrocyte images after treatment of ZPA@HA-ACVA-AZ NBs at 50 μg/mL and 400 μg/mL concentration using a microscope (scale bars: 50 μm)

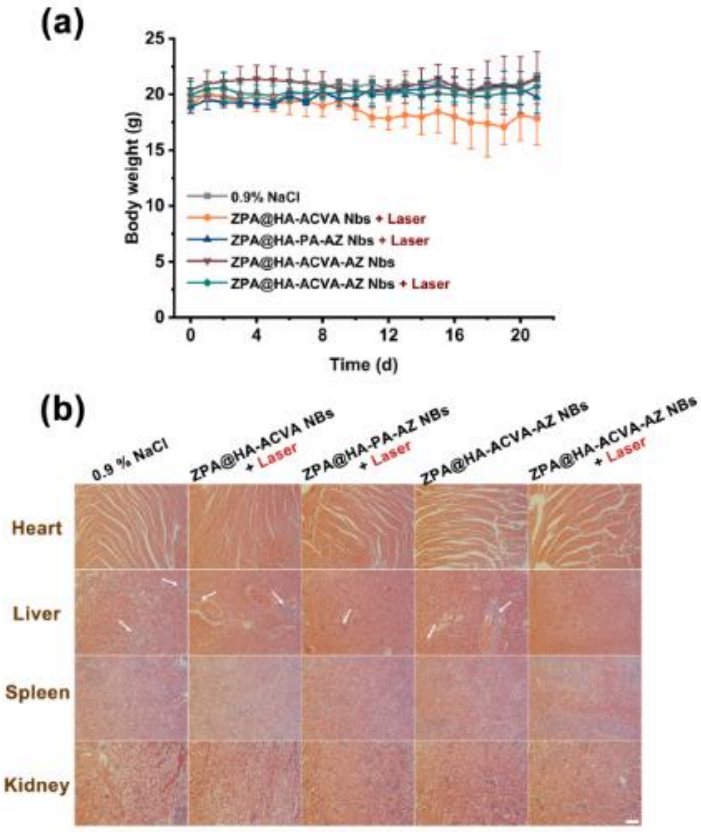

Fig. S23 a Body weight changes and **b** H&E images (on day 21) of normal tissues in balb/c mice bearing 4T1 tumor after systematic injection of different drug formulations (scale bars: 200 μm)

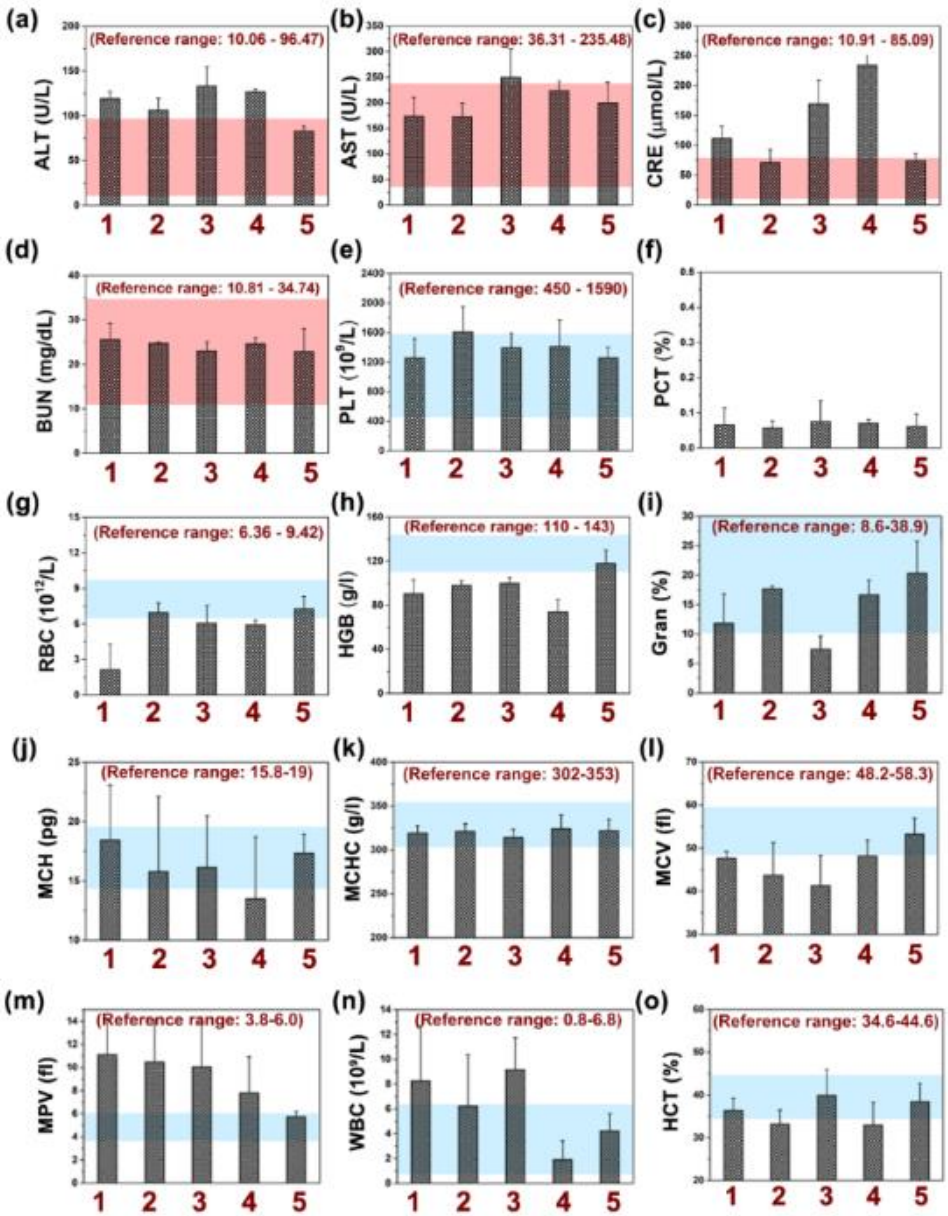

Fig. S24 The blood level of **a** ALT, **b** AST, **c** CRE, **d** BUN in plasma and **e-o** the routine blood examination on day 21 of balb/c mice bearing 4T1 tumors after systematic injection of different drug formulations. (1: 0.9% NaCl, 2: ZPA@HA-ACVA NBs + laser, 3: ZPA@HA-PA-AZ NBs + laser, 4: ZPA@HA-ACVA-AZ NBs, 5: ZPA@HA-ACVA-AZ NBs + laser)

Table S1 Characterization of HA-based amphiphilic lipoid.

Polymers	Feed molar ratio[a]		Calculated grafting degree[b]	
	ACVA-HDA or PA	AZ	ACVA-HDA or PA	AZ
HA-ACVA-*1*	20%	-	2.5%	-
HA-ACVA-AZ-*1*	20%	30%	3.2%	19.5%
HA-ACVA -*2*	50%	-	7.9%	-
HA-ACVA-AZ-*2*	50%	30%	8.1%	18.8%
HA-ACVA-*3*	70%	-	11.4%	-
HA-ACVA-AZ-*3*	70%	30%	11.9%	15.0%
HA-PA	50%	-	8.3%	-
HA-PA-AZ	50%	30%	8.1%	17.9%

[a] Feed molar ratio of ACVA-HDA, PA and AZ to the hydroxyl groups of the side chain of HA during the synthesis of HA-based amphiphilic polymers.

[b] Grafting degree of ACVA-HDA, PA and AZ on the side chain of HA calculated based on ^{1}H NMR spectra.

Table S2 Characterization of the blank HA-ACVA-AZ NBs and ZPA@HA-ACVA-AZ NBs prepared by different HA-based amphiphilic lipoids.

NBs	Size (nm)	PDI	Zeta potential (mV)	Entrapment efficiency %	Drug loading %
HA-ACVA-AZ NBs-*1*	251.74±30.97	0.103±0.01	-29.03±2.57	-	-
HA-ACVA-AZ NBs-*2*	271.83±22.31	0.149±0.01	-44.49±8.95	-	-
HA-ACVA-AZ NBs-*3*	241.73±32.17	0.325±0.01	-23.46±1.02	-	-
ZPA@HA-ACVA-AZ NBs-*1*	360.27±26.99	0.157±0.04	-30.04±3.12	73.06 %	6.81 %
ZPA@HA-ACVA-AZ NBs-*2*	297.99±21.89	0.126±0.03	-34.70±6.23	89.65 %	8.23 %

ZPA@HA-ACVA-AZ NBs-*3*	286.49 ±12.94	0.283 ±0.02	-25.64 ±5.49	72.86 %	6.79 %